

The microwave spectrum of a two-top peptide mimetic: The *N*-acetyl alanine methyl ester molecule

David F. Plusquellic^{a)}

Optical Technology Division, National Institute of Standards and Technology, Gaithersburg, Maryland 20899-8441

Isabelle Kleiner

Laboratoire Inter-Universitaire des Systèmes Atmosphériques, Université Paris 7 et Paris 12 et CNRS, 61 Avenue Charles de Gaulle, 94010 Créteil Cedex, France

Jean Demaison

Laboratoire de Physique des Lasers, Atomes et Molécules, UMR CNRS 8523, Université de Lille I, 59655 Villeneuve d'Ascq Cedex, France

Richard D. Suenram, Richard J. Lavrich, Frank J. Lovas, and Gerald T. Fraser

Optical Technology Division, National Institute of Standards and Technology, Gaithersburg, Maryland 20899-8441

Vadim V. Ilyushin

Institute of Radio Astronomy of NASU, Chervonopraporna Street 4, 61002 Kharkov, Ukraine

(Received 6 July 2006; accepted 10 August 2006; published online 14 September 2006)

The rotational spectrum of *N*-acetyl alanine methyl ester, a derivative of the biomimetic, *N*-acetyl alanine *N'*-methyl amide or alanine dipeptide, has been measured using a mini Fourier transform spectrometer between 9 and 25 GHz as part of a project undertaken to determine the conformational structures of various peptide mimetics from the torsion-rotation parameters of low-barrier methyl tops. Torsion-rotation splittings from two of the three methyl tops capping the acetyl end of the $-\text{NH}-\text{C}(=\text{O})-$ and the methoxy end of $-\text{C}(=\text{O})-\text{O}-$ groups account for most of the observed lines. In addition to the *AA* state, two *E* states have been assigned and include an *AE* state having a torsional barrier of $396.45(7) \text{ cm}^{-1}$ (methoxy rotor) and an *EA* state having a barrier of $64.96(4) \text{ cm}^{-1}$ (acetyl rotor). The observed torsional barriers and rotational constants of alanine dipeptide and its methyl ester are compared with predictions from Møller-Plesset second-order perturbation theory (MP2) and density functional theory (DFT) in an effort to explore systematic errors at the two levels of theory. After accounting for zero-point energy differences, the torsional barriers at the MP2/cc-pVTZ level are in excellent agreement with experiment for the acetyl and methoxy groups while DFT predictions range from 8% to 80% too high or low. DFT is found to consistently overestimate the overall molecular size while MP2 methods give structures that are undersized. Structural discrepancies of similar magnitude are evident in previous DFT results of crystalline peptides. © 2006 American Institute of Physics. [DOI: [10.1063/1.2348871](https://doi.org/10.1063/1.2348871)]

I. INTRODUCTION

Rotational spectroscopy has provided a wealth of structural, conformational, and torsional barrier information on small organic and inorganic molecules to guide the development and application of computational chemistry to problems in chemistry, physics, and materials science. Such spectroscopic data have been applied successfully to the development and testing of molecular force fields used in molecular mechanics modeling.¹ It has also been widely used to guide the optimization of the numerous density functionals for *ab initio* electronic structure calculations by means of comparisons made with highly precise and reliable experimental structural data on model systems.² Indeed, because of its unsurpassed computational efficiency, density functional

theory (DFT) is a major component of many quantum chemical packages with recent applications extending to periodic crystalline solids in the condensed phase environments.³

The increasing application of computational chemistry to problems in molecular biology, biotechnology, and nanotechnology is leading to new demands for validation data on systems which more closely mimic biological molecules in their conformational richness and functionality. Rotational spectroscopic data are generally lacking on such biomolecular mimetics, limiting the availability of “molecular standards” to validate the computational method selected to study the more complex biological system of interest. Alternatively, researchers have resorted to using results from higher level quantum chemistry calculations on model systems and/or experimental results from NMR and x-ray crystallographic studies on molecules containing functional groups related to the molecule of interest.⁴ Limiting the utility of the latter approach is the contamination of NMR and

^{a)} Author to whom correspondence should be addressed. Fax: 301-975-6991. Electronic mail: david.plusquellic@nist.gov

x-ray crystallography structural data by intermolecular interactions with the condensed-phase environment. These types of interactions may differ from the environment of interest or lead to optimizations in which the parameters are contaminated by undesired environmental contributions. Furthermore, because of the numerous density functionals that are currently available and the lack of any clear measure to select *a priori* the best functional for the system under study (particularly for strongly hydrogen bonded systems), comparisons with structural data of small isolated biomimetics provide a simple and reliable means for making such evaluations.

As one such example where system size prohibits a thorough evaluation of the optimal functional, predictions from force field (CHARMM¹) and density functional theory (DFT/PW91) have recently been reported for three different crystalline forms of trialanine that differ in β -sheet form and hydrolysis content.⁵ The observed sensitivity of the terahertz vibrational modes (which probe the incipient motions responsible for folding) to the hydrogen bonding network linking the peptide monomers and the cocrystallized water is dramatic. However, when compared with theoretical predictions using two functionals (PW91 and PBE), significant disagreement is found between the x-ray structural data and the terahertz absorption spectra at these levels of theory providing further motivation for the current study.

The discrepancies with theory suggest the need for further evaluation and refinement of functionals using more diverse (and complex) experimental data sets than the small molecule and hydrogen bonded complexes currently employed.² For protein structure, a functional group critical to these structural evaluations is the peptide bond linkage, $-\text{[NHCO]}-$. In addition to the methyl ester of alanine dipeptide investigated here, a large set now exists including the simplest peptide, formamide, H-[NHCO]-H ,⁶ and its derivatives, acetamide, H-[NHCO]-CH_3 ,⁷ *N*-methylformamide, $\text{CH}_3-\text{[NHCO]-H}$,⁸ *N*-methylacetamide $\text{CH}_3-\text{[NHCO]-CH}_3$,⁹ *N,N*-dimethylformamide, $(\text{CH}_3)_2-\text{[NCO]-H}$,¹⁰ *N*-methylpropionamide, $\text{CH}_3-\text{[NHCO]-CH}_2\text{CH}_3$,¹¹ methyl carbamate, H-[NHCO]-OCH_3 ,¹² and the ethyl acetamidoacetate molecule (EAA) or *N*-acetylglycine ethyl ester $\text{CH}_3-\text{[CONH]-CH}_2\text{C(=O)OCH}_2\text{CH}_3$.¹³ More recently, a few dipeptide derivatives, *N*-acetyl-alanine *N'*-methylamide or alanine dipeptide (AAMA), $\text{CH}_3-\text{[CONH]-CHCH}_3-\text{[CONH]-CH}_3$,¹⁴ and *N*-acetyl-proline *N'*-methylamide or proline dipeptide (APMA), $\text{CH}_3-\text{[CON]-CHC}_3\text{H}_6-\text{[CONH]-CH}_3$,¹⁵ were also studied.

In all of these studies, rotational spectroscopy has been used as a tool for conformer identification and molecular structure determination since different conformers have very different moments of inertia and, therefore, have different rotational spectra. Moreover, in all cases except formamide, at least one methyl group caps either the N-terminus end, $\text{CH}_3-\text{[NHCO]}-$, or the C-terminus end, $\text{CH}_3-\text{[CONH]}-$, of the peptide bond and torsional barriers are sufficiently low that additional splittings are observed. For example, in the formamide derivatives, the V_3 barriers range from 60 cm^{-1} (even 25 cm^{-1} for acetamide) to 100 cm^{-1} . These torsional

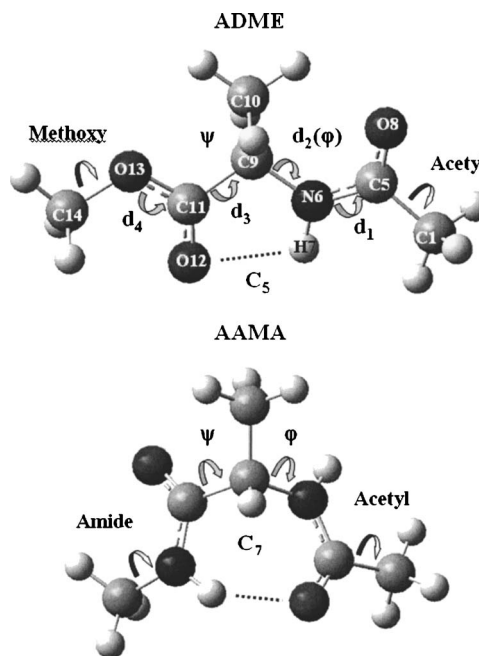


FIG. 1. Lowest energy structures of *N*-acetyl alanine methyl ester (AAME-top) and *N*-acetyl alanine *N'*-methyl amide (AAMA-bottom) at the MP2/cc-pVTZ level illustrating the intramolecular hydrogen bonding arrangements that define the C_5 and C_7 configurations, respectively. The atoms are numbered to be consistent with the dihedral angles given in Table IV. Tunneling splittings are observed only for the methyl groups indicated with arrows capping the $\text{CH}_3\text{C(=O)NH-}$ ends (acetyl), the $-\text{C(=O)OCH}_3$ end (methoxy), and $-\text{C(=O)NHCH}_3$ (amide) end.

splittings are much larger than those from, for example, the ethyl group where V_3 barriers typically range from 800 to 1200 cm^{-1} . When methyl caps an oxygen atom to form a methoxy group, $-\text{OCH}_3$, like in the methyl carbamate molecule, the barrier height is $\approx 400 \text{ cm}^{-1}$ and intermediate in magnitude.¹²

Increasingly complex biomimetics have also been studied using rotational spectroscopy including a few having two low barrier tops. For example, using a perturbative-based treatment that fits each of the torsional states separately, the microwave studies of AAMA (Ref. 14) and APMA (Ref. 15) have reported V_3 barriers of 81.6(1) and 98.5(2) cm^{-1} for the AAMA-¹⁴N₂ and 337.6(5) and 80.1(1) cm^{-1} for APMA-¹⁴N₂, respectively. The spectrum of *N*-methylacetamide⁹ (studied using a global method that fits all torsion-rotational states together) shows similar barriers of 73.468(51) and 79.062(93) cm^{-1} , respectively. In nearly all cases, analysis of the torsion-rotation splittings permits an accurate determination of the methyl group(s) torsional barrier and its orientation in the molecule, following the method described in Ref. 14. The torsional barriers and orientation angles provide rigorous points of comparison with force field and *ab initio* theories.

The present work is concerned with the rotational spectrum of the methyl ester derivative of AAMA, *N*-acetyl-alanine methyl ester (AAME), where the $\text{CH}_3-\text{[NHCO]}-$ fragment has been substituted by the group, $\text{CH}_3-\text{C(=O)-O-}$, shown in the top panel of Fig. 1. We expect the methyl rotor group attached to the alpha carbon of alanine to be hindered by a barrier that is too large to give

rise to observable splittings in the spectrum (*vide infra*). Therefore, this molecule is an example of an alanine derivative having resolvable splitting from two methyl tops.

One purpose of the present work is to compare the results of two different one-top fitting models: the effective perturbation treatment described in Ref. 14 and the rho-axis method (RAM) global approach described in Refs. 13 and 16. These two methods have both been used for a number of one-top methyl-rotor molecules and compared previously in the case of the ethyl acetamidoacetate molecule (EAA) which has two low energy conformers, one with all the heavy atoms lying in plane (C_s global fit program) and one with the ethyl group folding out of plane (C_1 global fit program).^{13,16} The focus here is to compare the results of these two one-dimensional (1D) fitting approaches to arrive a better estimate of the experimental uncertainties associated with the methyl top orientations (and other torsional parameters) of a two-top molecule.

A second focus of this work is to explore the accuracy of quantum chemical calculations for determinations of biomolecular structure and methyl torsional barriers. For this purpose, we include the results from AAMA, since the lowest energy conformer has a C_7^q configuration characterized by an intramolecular hydrogen bond between adjacent peptide linkages in Fig. 1 (bottom). This configuration is in contrast to the lowest energy extended chain or C_5 conformation of AAME found here in Fig. 1 (top), thereby providing comparison data for two different structural motifs. We also use these two systems to examine theoretical contributions to the torsional barriers from vibrational zero-point effects and the next higher-order Fourier component in the torsional potential energy surfaces.

II. EXPERIMENT

Like all peptide related compounds, AAME is a solid at room temperature and requires heating to produce sufficient vapor pressure for study in the gas phase. It was expected that the methyl ester functionality on the end of the molecule would make this particular compound more volatile than the AAMA previously studied.¹⁴ However, it was also expected that thermal decomposition might still occur so a Silcosteel™ coated reservoir nozzle was used. Several exploratory survey scans were made at increasingly higher temperatures using a mini Fourier transform microwave (FTMW) spectrometer at NIST.¹⁷ The first transitions were observed when the reservoir temperature reached approximately 150 °C. Once a stable spectrum was obtained, a complete set of measurements was performed in the frequency range between 9 and 25 GHz.

III. RESULTS

A. Spectral assignments

The energy level diagram of the expected torsional level splittings of AAME is shown in Fig. 2. The two-top notation described in Ref. 9 is used here where the two letters, AA, AE, EA, and EE, indicate the symmetry species of the wave function with respect to the nuclear-permutation-inversion group of two methyl tops; AA, AE, EA, and EE correspond to

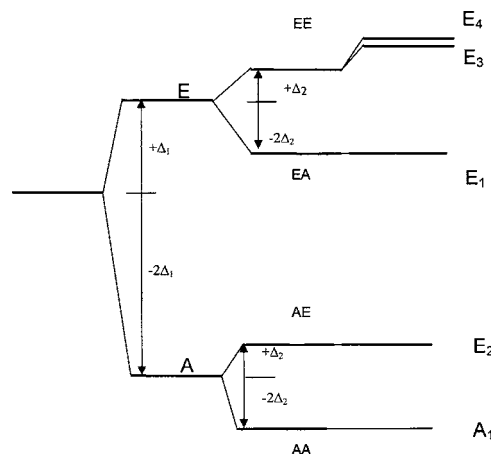


FIG. 2. The three sets of internal splittings in AAME (the figure is not done at the exact energy scale) for $J=K=0$; 1. (AA,EA) $V_3=65.6$ cm^{-1} , low barrier case: $\Delta_1 \approx 2$ cm^{-1} ; 2. (AA,AE) $V_3=399.2$ cm^{-1} , high barrier case: $\Delta_2 \approx 0.01$ cm^{-1} ; 3. (AA,EE) not treated here. The level on the left is first split into A and E torsional components by the acetyl methyl rotor. Each of these levels is further split into two levels by the methoxy methyl top. The EE level is finally split into two levels due to the top-top interaction (not treated here). The energy labels A_1, A_2, E_1, E_2, E_3 , and E_4 in column 4 use the G_{18} permutation-inversion species notation and the AA, AE, EA, and EE notations in column 2 refers to the notation $C_3^1 \otimes C_3^2$ where the superscripts indicate the acetyl and methoxy methyl tops, respectively (for a complete description of the group theory, see also Table I and Fig. 3 of Ref. 9).

A_1, E_2, E_1 , and E_3/E_4 , respectively, in the permutation-inversion group G_{18} . It was anticipated from previous studies of acetyl methyl tops capping peptide bonds^{7,9,13-15} that a large torsional splitting would occur for this group. This splitting is labeled as Δ_1 in Fig. 2 and identified throughout this work as the (AA,EA) state set. Conversely, the expected high barrier of the methoxy top would give a smaller splitting labeled as Δ_2 in Fig. 2 and identified here as the (AA,AE) state set. The presence of resolvable splittings from two tops requires also transitions from a third (AA,EE) state set and the additional splitting associated with the EE state also shown in the figure.

The MW spectrum from survey scans of AAME is shown in the upper trace of Fig. 3. It was rather straightfor-

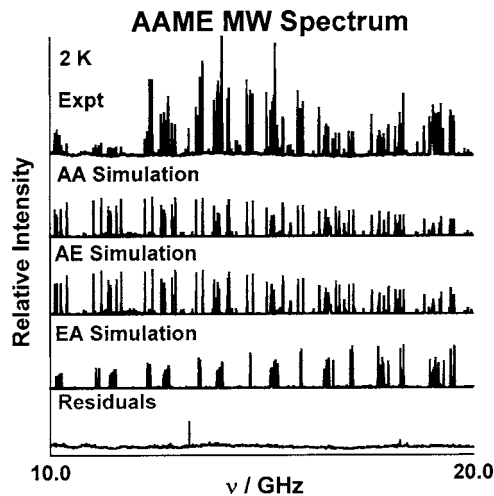


FIG. 3. Observed and calculated spectra for the 10–20 GHz frequency range.

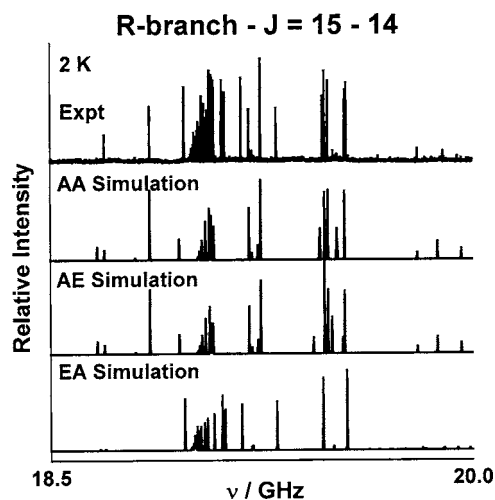


FIG. 4. Observed and calculated spectral region containing the $J=15-14$ transitions.

ward to assign the gross features of the AA state since the overall spectrum appears to be that of a prolate rotor having a -type selection rules. The high K_{-1} a -type, R -branch transitions occur in a regular pattern, spaced by approximately $(B+C)$ where B and C are the rotational constants. The R -branch “pileups” are easily visible in Fig. 3 with a spacing of about 1.6 GHz. In addition to the methyl torsional splittings, AAME contains one ^{14}N nucleus and, therefore, nuclear quadrupolar coupling will result in a hyperfine pattern for each rotational line. The hyperfine structure of the AA state was modeled in first order and assigned using features of the graphical user interface program, JB95.^{14,18} The assigned line set was then fit using a second-order nuclear quadrupole Hamiltonian. Rotational transitions obeying a -type, b -type, and c -type selection rules were observed and fit to a standard deviation of 1.3 kHz, well within the experimental uncertainty of 4 kHz. The best-fit rotational and nuclear quadrupole hyperfine constants for the AA state are given in Table I. The simulated spectrum is shown below the experimental traces in Figs. 3 and 4.

Located near many of the AA-state lines were transitions having very different hyperfine splitting patterns. These transitions were attributed to the AE state of the methoxy methyl rotor. It was straightforward to model the torsion-rotation perturbations of this state using the principal axis method.¹⁹ However, locating and assigning the third set of transitions associated with the low barrier EA state was much more difficult, requiring first, reasonable estimates of parameters and second, the use of closed loops to confirm assignments. Furthermore, to obtain reliable line centers, the AA-state hyperfine parameters were used to model and assign in first order the nuclear quadrupole structure of the EA and AE states. As evident from the standard deviations reported in Table I, this first-order procedure worked extremely well. Simulated spectra of the EA and AE states predicted using JB95 are shown in Figs. 3 and 4.

The experimental residual trace where the AA-, AE-, and EA-state transitions have been removed is shown at the bottom of Fig. 3. At the signal-to-noise ratio of these measurements, only a few unassigned transitions remain, suggesting

that only one conformational isomer is present in the jet-cooled expansion. The few remaining lines near the noise floor are likely associated with the fourth (EE) state and not treated further here using our one-top programs.

B. Least-squares fits

For the perturbative-based method, rotational transitions of the AA torsional state are fitted separately from transitions of the AE and EA torsional states.¹⁹ The resulting constants are then compared in pairs for the (AA,AE) and (AA,EA) sets using perturbation theory applied to a one-top rotation Hamiltonian to determine the barriers and the methyl rotor axis directions.¹⁴ In the so-called RAM, the two sets, (AA,AE) and (AA,EA), are each fitted together also using a one-top formalism (designated here as the global fit method) and the barrier height as well as other torsional parameters are determined directly as floated parameters.¹⁶

Using the perturbative-based approach as implemented in the JB95 program,¹⁸ the 58, 65, and 72 rotational lines assigned to the AA, EA, and AE states were fitted to 1.3, 1.9, and 2.1 kHz, respectively. The best-fit parameters and uncertainties (type A, $k=1$ or 1σ)²⁰ are given in Table I. The AA state was fitted to a Watson A -reduction asymmetric rotor Hamiltonian (representation I'). The EA-state transitions of the acetyl methyl top were fitted in the “rho-axis” frame by adding a linear Coriolis term, $D'_a\mathbf{P}'_a$, three off-diagonal moment of inertia operators, $E_{\alpha\beta}(\mathbf{P}_\alpha\mathbf{P}_\beta + \mathbf{P}_\beta\mathbf{P}_\alpha)$ with $\alpha, \beta = a, b, c$, and a few additional terms in higher powers of \mathbf{P} . We note that one of the off-diagonal cross terms (E_{ac}) has been fixed to the value given by the minimum standard deviation as discussed elsewhere.¹⁴ Indeed, as already pointed out in Refs. 13 and 14, all three of the off-diagonal cross products, E_{ab} , E_{ac} , and E_{bc} , cannot be simultaneously determined since one of them can be removed by an appropriate rotation about the ρ axis. Because of the larger torsional barrier of the methoxy top, fits of the AE state using JB95 were performed in two different reference frames. One fit was performed in the “rho-axis” frame using the D'_a , E_{ab} , and E_{ac} terms described above and a second fit was done in the principal axis system using the three linear operators, $D_a\mathbf{P}_a$, $D_b\mathbf{P}_b$, and $D_c\mathbf{P}_c$. In the former case, the rotational constants were only poorly determined while in the latter, they were well fit. Therefore, the principal axis frame results are given in Table I. We note, however, that the two linear coefficients, D_b and D_c , have large uncertainties and, hence, the propagated uncertainties associated with the rotor axis angles are also large. These uncertainties did not decrease when fits were performed in the rho-axis frame.

Using the global fit approach available in the C_1 program,^{13,16} each torsional state pair, (AA,AE) or (AA,EA), was fitted together. The standard deviations of the fits given in Table II are of the same quality as the perturbative fits and within the experimental line uncertainty of 4 kHz, i.e., 2.5 kHz for the 123 lines belonging to the (AA,EA) set and 1.8 kHz for the 130 lines belonging to the (AA,AE) set. Table II gives the best-fit parameters obtained for the two state pairs.²¹ Here, too, the acetyl methyl top presents no particular problem when fitting two of the off-diagonal iner-

TABLE I. Torsion-rotation parameters of the *AA* state, *EA* state (acetyl rotor), and *AE* state (methoxy rotor) from JB95 fits of Fourier transform microwave transitions. The nuclear quadrupole parameters fit to the *AA* state are given in the lower part. Type-A standard uncertainties (Ref. 20) (i.e., $k=1$ or 1σ) from the least-squares fits are given in parentheses.

| Parameter ^a | Operator | <i>AA</i> state ^b | <i>EA</i> state ^b | <i>AE</i> state ^b |
|-------------------------------|---------------------------------------|------------------------------|------------------------------|------------------------------|
| <i>A</i> (MHz) | P_a^2 | 3011.890 9(2) | 2883.967(1) | 3011.685 3(2) |
| <i>B</i> (MHz) | P_b^2 | 670.727 22(5) | 753.5632(9) | 670.725 68(7) |
| <i>C</i> (MHz) | P_c^2 | 596.329 88(7) | 620.8455(1) | 596.330 08(8) |
| <i>D_a</i> (MHz) | P_a | ... | 1126.632(1) | 6.441 6(5) |
| <i>D_b</i> (MHz) | P_b | ... | ... | -0.65(12) |
| <i>D_c</i> (MHz) | P_c | ... | ... | -0.093(1) |
| <i>E_{ab}</i> (MHz) | $P_a P_b + P_b P_a$ | ... | 440.753(2) | ... |
| <i>E_{ac}</i> (MHz) | $P_a P_c + P_c P_a$ | ... | 214.9584 ^{fixed} | ... |
| <i>E_{bc}</i> (MHz) | $P_b P_c + P_c P_b$ | ... | 59.2224(3) | ... |
| Δ_{JK} (kHz) | $-P^2 P_a^2$ | -0.072(2) | -0.814(5) | -0.069(3) |
| Δ_J (kHz) | $-P^4$ | 0.024 7(1) | 0.0397(3) | 0.024 9(2) |
| Δ_K (kHz) | $-P_a^4$ | 3.88(3) | 4.70(2) | 3.83(1) |
| δ_J (kHz) | $-2P^2(P_b^2 - P_c^2)$ | 0.000 24(6) | 0.0072(4) | ... |
| δ_K (kHz) | $-[P_a^2(P_b^2 - P_c^2)]$ | 0.45(2) | -0.11(1) | 0.46(2) |
| <i>G_a</i> (kHz) | P_a^3 | ... | -182.2(1) | -1.49(3) |
| <i>G_{aab}</i> (kHz) | $P_a^2 P_b + P_a P_b P_a + P_b P_a^2$ | ... | 2.4(1) | ... |
| <i>G_{baa}</i> (kHz) | $P_b^2 P_a + P_b P_a P_b + P_a P_b^2$ | ... | -0.47(6) | ... |
| <i>L_a</i> (kHz) | P_a^5 | ... | 0.020(2) | ... |
| <i>eQq_{aa}</i> (MHz) | | 2.032(3) | c | c |
| <i>eQq_{bb}</i> (MHz) | | 1.072(3) | c | c |
| <i>eQq_{cc}</i> (MHz) | | -3.104(3) | c | c |
| σ_{rms} (kHz) | | 1.3 | 1.9 | 2.1 |
| | | 58 lines, 8 par. | 65 lines, 16 par. | 72 lines, 11 par. |

^aParameter names and units are given in the first column; the operators which these parameters multiply in the torsion-rotation Hamiltonian are given in column two. $[A, B] = AB + BA$.

^bAcetyl and methoxy tops are methyl rotors capping the *N*-acetyl group $\text{CH}_3\text{C}(=\text{O})\text{NH}$ - (low barrier case) and methoxy group, $-\text{C}(=\text{O})\text{OCH}_3$ (high barrier case) and correspond to the splittings of the (*AA*, *EA*) and (*AA*, *AE*) datasets, respectively.

^c*AA*-state parameters used in the first-order approximation to determine the *EA*- and *AE*-state rotational line centers. See text for details.

tial cross terms (namely, E_{ab} and E_{bc}) whereas in the high barrier case, these two terms are poorly determined and no higher-order terms could be determined.

Structural data related to the acetyl and methoxy rotors were obtained in the following way. From fits performed in the rho-axis frame using either method, the principal axis rotational constants were obtained from diagonalization of the inertia tensor involving one or more of the off-diagonal cross products. For the perturbative approach and in either reference frame, the “infinite barrier” constants, A_R , B_R , and C_R , were obtained from the average of the *A*- and *E*-state principal axis values after applying second-order corrections given by Eqs. (2) and (6) of Ref. 14. The methyl rotor axis angles relative to the principal axis system, torsional barriers, and other rotor constants were calculated using the separate program.¹⁴ These parameters together with the corresponding values from the global fit method are summarized in Table III for both tops.

As evident from Table III, the rotational constants obtained from the two methods agree to within 0.01%–0.1%. The torsional barriers determined for the acetyl and methoxy methyl rotors are 64.96(4) and 396.45(7) cm^{-1} using the C_1 -RAM program and 66.35(5) and 402(4) cm^{-1} using the JB95 program, respectively. These differences are within a

few percent and similar to those found in the study of ethyl acetamidoacetate.¹³ The discrepancies are, however, larger than the standard deviation of the parameters by an order of magnitude and likely a result of systematic errors in the models. The same holds true for the torsional parameter, ρ .

By far, the largest discrepancies between the methods appear in the rotor axis angles of the methoxy top, differing by as much as a few degrees (although still within the propagated experimental uncertainties). This is in contrast to the much smaller differences of 0.2° or less for the acetyl methyl top. In the high barrier case, it is more difficult to get the torsion-rotational parameters with the same precision as for the low barrier case, since the torsional splittings are small in the ground torsional state. This led to a situation when both F and V_3 cannot be simultaneously determined with the limited data set available here for the ground torsional state only. Furthermore, from the fits in the rho-axis frame using either method, the constants A , B , and E_{ab} are highly correlated and this led to large uncertainties in the values of the torsional angles. We also cannot rule out the possibility that top-top interactions could likely play a larger role for the small torsional splittings of the methoxy group making our one-top models less reliable. Finally, the peptide bond may become slightly nonplanar during methyl torsional motion.

TABLE II. Torsion-rotation parameters from C₁-RAM global fits of Fourier transform microwave transitions. (Complete least-squares fit outputs containing all assigned transitions, observed minus calculated residuals, etc., can be found in the journal's supplementary material.) Type-A standard uncertainties (Ref. 20) (i.e., $k=1$ or 1σ) from the least-square fits are given in parentheses.

| Parameter ^a | <i>nlm</i> | Operator | (<i>AE</i> , <i>EA</i>) states ^b | (<i>AA</i> , <i>AE</i>) states ^c |
|-----------------------------|------------|---|---|---|
| V_3 (cm ⁻¹) | 220 | $\frac{1}{2}(1 - \cos 3\gamma)$ | 64.96(4) | 396.45(7) |
| F (cm ⁻¹) | | P_γ^2 | 5.341(2) | 5.30 ^c |
| ρ | 211 | $P_\gamma P_a$ | 0.013 375(1) | 0.017 68(2) |
| A (MHz) | 202 | P_a^2 | 2890.401 6(9) | 2992.0(5) |
| B (MHz) | | P_b^2 | 774.16(6) | 689.2(7) |
| C (MHz) | | P_c^2 | 600.45(6) | 597.5(5) |
| E_{ab} (MHz) | | $P_a P_b + P_b P_a$ | -491.088(7) | -214.(3) |
| E_{ac} (MHz) | | $P_a P_c + P_c P_a$ | 0 ^{fixed} | 0 ^{fixed} |
| E_{bc} (MHz) | | $P_b P_c + P_c P_b$ | 15.831 4(2) | 9.(2) |
| G_V (MHz) | 422 | $P_\gamma^2 P^2$ | -0.048 2(3) | 0.013(3) |
| c_2 (MHz) | | $(1 - \cos 3\gamma)(P_b^2 - P_c^2)$ | 1.2(1) | ... |
| c_1 (MHz) | | $2P_\gamma^2(P_b^2 - P_c^2)$ | 0.044(5) | ... |
| d_{ab} (MHz) | | $(1 - \cos 3\gamma)(P_a P_b + P_b P_a)$ | 1.75(2) | ... |
| Δ_J (kHz) | 404 | $-P^4$ | ... | 0.023 08(9) |
| Δ_{JK} (kHz) | | $-P^2 P_a^2$ | 1.04(1) | -0.148(3) |
| Δ_K (kHz) | | $-P_a^4$ | 1.63(3) | 3.994(9) |
| δ_J (kHz) | | $-2P^2(P_b^2 - P_c^2)$ | -0.013 4(2) | -0.000 71(8) |
| δ_K (kHz) | | $-[P_a^2(P_b^2 - P_c^2)]$ | 0.453(8) | 0.29(1) |
| D_{abK} (kHz) | | $P_a^3 P_b + P_b P_a^3$ | 2.16(2) | ... |
| σ_{rms} (kHz) | | $A+E/A/E$ | 2.5/1.6/3.1 | 1.8/1.4/2.0 |
| | | $A+E$ | 123 lines, 17 par. | 130 lines, 14 par. |

^a(Parameter names and units are given in the first column. The operators which these parameters multiply in the torsion-rotation Hamiltonian are given in column three, except for F , ρ , and A which appear in the Hamiltonian in the form $F(P_\gamma - \rho P_a)^2 + AP_a^2$. Column two contains an *nlm* ordering scheme (Ref. 9) for these operators. [A, B]= $AB+BA$) of the *AA* state, *EA* state (acetyl rotor), and *AE* state (methoxy rotor).

^bAcetyl and methoxy tops are methyl rotors capping the *N*-acetyl group, CH₃C(=O)NH- (low barrier case) and methoxy group, -C(=O)OCH₃ (high barrier case) and correspond to the splittings of the (*AA*, *EA*) and (*AA*, *AE*) data sets, respectively.

^cThe F and V_3 values could not be determined simultaneously in the high barrier case. F was held fixed to the value corresponding to a value commonly accepted for methyl rotors.

Higher-order terms are needed to model such behavior but were not reliably determined in the high barrier case in contrast to the low barrier fits where five higher-order terms could be well determined (see c_1 , c_2 , d_{ab} , D_{abK} , and G_V in Table II).

IV. DISCUSSION

The gas-phase model peptides examined here and elsewhere provide quantitative structural data to evaluate the accuracy and overall deficiencies of *ab initio* methods. The importance of having such data becomes clear from the poor predictive quality of terahertz vibrational spectra of condensed-phase crystalline peptides.⁵ While computations of such large systems are now within the scope of software packages employing density functional theory, a systematic evaluation is problematic because of (i) the time required per calculation and (ii) the impact of the environment. Evaluating functionals based on gas-phase model systems is therefore a necessary first step before predictions on complex condensed-phase crystalline peptides can be refined.

In this section, we begin with the experimental determination of the structural parameters from the torsional state analyses of AAME whereupon a definitive conformational assignment is made following a full conformational search.

The results previously reported for AAMA are included in this discussion because of the different conformation forms exhibited by these two systems. Both molecules are small enough to apply high level quantum chemical methods that include electron correlation with large basis sets. Finally, we focus on comparisons of the observed structural data and methyl torsional barriers with theoretical predictions from Moller-Plesset perturbation theory (MP2) and density functional theory (DFT) for a few of the most common functionals used for hydrogen bonded systems.

A. Structural parameters

The experimentally determined rotational constants, A_R , etc., reported for each rotor in Table III were obtained after correction for the effects of internal rotation. However, for a valid comparison with the static structures determined from theory, the experimental parameters must be corrected for dynamical contributions from both rotors. The corrections are most easily evaluated from the second-order perturbation theory. For example, the second-order corrections to the A constants in Table I are (+13.4, -6.0) and (+0.14, -0.07) MHz for the (*AA*, *EA*)- and (*AA*, *AE*)-state pairs, respectively, and are reported individually as A_R , etc., and together as A_{RR} , etc., in Table III. While simultaneous rotor

TABLE III. Comparison between the rotational constants, methyl torsional parameters, barriers, and angles of the acetyl and methoxy methyl rotors obtained from the two fitting procedures.

| | Global fit ^a | | JB95 ^b | |
|---|-------------------------|-----------------------|---------------------------|--------------------------|
| | (AA, EA) states | (AA, AE) states | (AA, EA) states | (AA, AE) states |
| A_R (MHz) ^c | 2998.8(1) | 3011.7(1) | 2998.2(7) ^d | 3011.755(5) ^d |
| B_R (MHz) ^c | 669.23(6) | 670.65(2) | 670.05(8) ^d | 670.7261(5) ^d |
| C_R (MHz) ^c | 596.97(2) | 596.25(2) | 596.29(2) ^d | 596.3300(2) ^d |
| ΔI ($\mu\text{\AA}^2$) ^e | -77.12 | -73.78 | -75.27 | -73.80 |
| $B_R + C_R$ (MHz) | 1266.20(8) | 1266.9(4) | 1266.33(9) | 1267.056(4) |
| A_{RR} (MHz) ^f | 2998.8(2) | | 2998.1(7) | |
| B_{RR} (MHz) ^f | 669.23(6) | | 670.05(8) | |
| C_{RR} (MHz) ^f | 596.97(2) | | 596.29(2) | |
| E_{ab} (cm^{-1}) ^g | -0.016 380 9(2) | -0.007 14(9) | -0.014 701 9(1) | 0 ^{fixed} |
| E_{bc} (cm^{-1}) ^g | 0.000 528 077(6) | 0.000 31(6) | 0.001 975 4(1) | 0 ^{fixed} |
| E_{ac} (cm^{-1}) ^g | 0 ^{fixed} | 0 ^{fixed} | 0.007 17 ^{fixed} | 0 ^{fixed} |
| ρ ^h | 0.0133 75(1) | 0.017 68(2) | 0.013 36(5) | 0.017 19(1) |
| V_3 (cm^{-1}) | 64.96(4) | 396.45(7) | 66.35(5) | 402(4) |
| F (cm^{-1}) ^h | 5.341(2) | 5.30 ^{fixed} | 5.30 ^{fixed} | 5.30 ^{fixed} |
| θ_a ($^\circ$) | 44.86(1) | 22.5(1.5) | 44.94(5) | 25.0(7.7) |
| θ_b ($^\circ$) | 46.75(1) | 67.7(1.0) | 46.59(5) | 65.2(8.5) |
| θ_c ($^\circ$) | 80.36(1) | 87.0(3.5) | 80.58(5) | 86.4(1.2) |

^aGlobal fits in the rho-axis frames (RAM) as described in Ref. 13. Type-A standard uncertainties (Ref. 20) (i.e., $k=1$ or 1σ) are given, as determined from the least-squares fit.

^bPerturbation based fits using JB95 by fitting the three torsional states separately. Type-A standard uncertainties (i.e., $k=1$ or 1σ) are given, as determined from the least-square fit and propagation of errors.

^cRotational parameters A_R , B_R , and C_R where $A_R = h^2/2I_a$, etc., are reported in the principal axis system after diagonalization of the inertia tensor.

^dAverage of AA- and EA or AE-state second-order-corrected rotational constants, i.e., $\frac{1}{2}(A_R^A + A_R^E)$, etc.

^eInertial effect $\Delta I = 505\,379(1/C - 1/A - 1/B)$.

^f A_{RR} , etc., represent rotational constants corrected to second order for both rotors. Error bars are type B (Ref. 20), $k=1$, and are assessed based on the contributions determined from perturbation theory when greater than the (AA, EA)-state uncertainties.

^gParameters multiplying ($P_a P_b + P_b P_a$) for E_{ab} , ($P_b P_c + P_c P_b$) for E_{bc} , ($P_a P_c + P_c P_a$) for E_{ac} , respectively (see Tables I and II).

^h F and ρ appear in the RAM Global fit Hamiltonian in the form $F(P_\gamma - \rho P_a)^2$.

corrections are not readily available using the global fit procedure, we note that contributions from the methoxy rotor (AE state) are small, amounting to 0.14 MHz or less. Therefore, for the global fit case, the A_{RR} , etc., constants reported in Table III are those determined for the (AA, EA)-state pair with expanded uncertainties conveying potential contributions from the methoxy rotor. In every case, the “rigid rotor” constants obtained from the two fitting procedures are within ± 1 MHz.

B. Conformational searches of AAME

Since no prior theoretical studies have been performed on AAME, conformational searches were first performed to identify the lowest energy forms. Starting geometries were defined by rotating about the dihedral angles, d_1 , d_2 , d_3 , and d_4 shown in Fig. 1 by 60° . Full geometry optimizations were performed on these initial forms using DFT as implemented in GAUSSIAN 03 program suite.²² The hybrid functional B3LYP (Becke’s three parameter functional²³ employing the Lee, Yang, and Parr correlation functional²⁴) and the 6-31G(d) basis set was chosen for its known reliability for predicting structures and relative energies.²⁵ Thirteen stable

conformers were located. The optimized values of the dihedral angles and relative energies are given in Table IV.

To further confirm the energy order, single point calculations were performed on the five lowest energy forms at the G3MP2B3 level of theory.²⁵ This is a compound method for calculating total energies of large molecules. It was assessed on a total of 299 energies and gave an average absolute deviation of 0.99 kcal/mol for the values reported in Table IV. Conformer A was again found to be lowest in energy by more than 2 kcal/mole, further supporting the observed absence of additional lines from other conformers at the temperature of our source (150°C).

The four lowest energy forms all have a *trans* peptide bond configuration as indicated by the small values of d_1 in Table IV. Of the four lowest energy forms, conformer A is an extended, almost linear chain with an intramolecular hydrogen bond characterizing a five-membered ring. This conformer is different from the C_7^{eq} form of AAMA and more closely resembles the second most stable form predicted for AAMA.¹⁴ The important structural distinctions of AAME and AAMA are shown in Fig. 1. Replacement of the NH-CH₃ group with the methyl ester group, O-CH₃, re-

TABLE IV. Lowest energy conformational structures at the B3LYP/6-31G(*d*) and G3MP2B3 levels of theory. Energies are specified relative to conformer *A* in kcal/mol.

| | Peptide bond | d_1^a (deg) | d_2^a (deg) | d_3^a (deg) | d_4^a (deg) | B3LYP/ 6-31G(<i>d</i>) ^b (kcal/mol) | G3MP2B3 ^b (kcal/mol) |
|-----------------------|--------------|------------------|------------------|------------------|------------------|--|------------------------------------|
| <i>A</i> ^a | <i>trans</i> | 7.1 | -157.4 | -9.0 | -0.4 | 0.0 | 0.0 |
| <i>B</i> | <i>trans</i> | 2.9 | -153.0 | 171.1 | -0.6 | 2.485 | 2.295 |
| <i>C</i> | <i>trans</i> | -8.3 | 51.5 | -146.9 | 5.0 | 4.129 | 2.556 |
| <i>D</i> | <i>trans</i> | -16.5 | 57.5 | 29.0 | -2.0 | 4.374 | 3.037 |
| <i>E</i> | <i>cis</i> | -175.4 | -147.2 | -20.1 | -0.6 | 4.763 | 4.549 |
| <i>F</i> | <i>cis</i> | -173.2 | -79.4 | 111.5 | -1.4 | 5.447 | |
| <i>G</i> | <i>cis</i> | 175.3 | 61.8 | -13.8 | -0.5 | 8.384 | |
| <i>H</i> | <i>trans</i> | 1.7 | -155.2 | -26.0 | 169.9 | 8.603 | |
| <i>I</i> | <i>cis</i> | -178.0 | -149.8 | -30.4 | 172.3 | 14.201 | |
| <i>J</i> | <i>trans</i> | 9.2 | 51.5 | -132.6 | -172.9 | 14.954 | |
| <i>K</i> | <i>trans</i> | -5.1 | -66.2 | 146.3 | 175.1 | 15.757 | |
| <i>L</i> | <i>trans</i> | -15.5 | 71.8 | -12.3 | 174.1 | 16.359 | |
| <i>M</i> | <i>cis</i> | 179.2 | -69.0 | 138.3 | 178.6 | 16.535 | |

^a d_1 (C1–C5–N6–H7), d_2 (C5–N6–C9–C11), d_3 (N6–C9–C11–O12), and d_4 (O12–C11–O13–C14) are the dihedral angles corresponding to the atom numbering in Fig. 1.

^bAbsolute energies are -515.715 74 hartrees and -514.974 138 hartrees at the B3LYP/631G(*d*) and G3MP2B3 levels of theory, respectively.

moves the proton donor group of AAMA thereby eliminating the intramolecular hydrogen bond characterizing the C_7^{eq} form. Hence, the Ramachandran angles, φ and ψ , that define these two forms resemble two different secondary structural motifs. The C_5 form is similar to an extended β -sheet structure having $\varphi \approx -159^\circ / \psi \approx +171^\circ$ while the C_7^{eq} is similar to that of the γ turn with $\varphi \approx -82^\circ / \psi \approx +75^\circ$.

C. Structural comparisons with theory

Full geometry optimizations were performed on the lowest energy conformers of AAME and AAMA using second-order Møller-Plesset perturbation theory²⁶ and the correlation-consistent polarized triple zeta basis set²⁷ (MP2/cc-pVTZ). DFT calculations were performed using two different program suites. Optimized geometries were obtained using the hybrid functional B3LYP/cc-pVTZ available in GAUSSIAN03.²² Additional DFT calculations were performed using the DMOL3 software suite which is capable of handling optimizations of crystalline solids. The latter calculations included all electrons and made use of a double numerical plus polarization (DNP) atomic orbital basis set (equivalent to a double ζ) and the functionals, PW91 (Ref. 28) and HCTH.²⁹ In each case, a harmonic frequency analysis was performed to confirm that the optimized geometry represented the true equilibrium structure.

A summary of the optimized parameters of AAME and AAMA is given in Tables V and VI, respectively. For ease of comparison with experiment, the parameters are specified as differences relative to the experimental values. For AAME, the experimental values were determined from the average of the two methods reported in Table III with experimental uncertainties representing the one-half the difference between the two methods. The rotor axis angles are of particular significance in these comparisons since these parameters are sensitive to the overall shape of the peptide along the soft torsional surfaces defined in large part by the strength of the

intramolecular hydrogen bond. For the theoretical structures, this axis is defined as a vector from the center of mass of the three methyl hydrogens to the methyl carbon atom to best account for the calculated asymmetry of the methyl group. The orientation of this vector is specified relative to the principal axis frame by the magnitudes of the (direction cosine) angles. A full discussion of the torsional barrier determinations from theory is given in the next section.

In general, the predicted rotational constants and rotor axis angles given in Tables V and VI are in good agreement with experiment for both AAME and AAMA. The calculated rotational constants are within 5% for AAME and 4% for AAMA and all angles are less than 4° . Notice also that the experimental uncertainties determined from the two fitting methods are typically much smaller than the discrepancies with theory. The only exception occurs for angles of the methoxy rotor of AAME for the reasons discussed above.

There are also some clear trends within each level of theory. For example, in nearly every case, DFT methods predict rotational constants that are too small compared to experiment while the MP2 values tend to overestimate them. Since the inertial parameters are inversely related to the rotational constants, the MP2 and DFT methods give overall structures that are smaller and larger than observed, respectively. The overestimated sizes predicted by DFT also have some bearing on results reported for the parallel and antiparallel β -sheet forms of crystalline trialanine.⁵ For example, at the DFT/PW91 level of theory, the majority of the hydrogen bond distances (measured as heavy atom separations) were underestimated by as much as 0.5 Å relative to the x-ray crystal data. It was not clear from this work whether the main source of error was from intramolecular interactions or from many body effects associated with the vast network of intermolecular hydrogen bonds. However, when the rotational constants of the two asymmetric molecules of the P21 (parallel) and C2 (antiparallel) unit cells are compared with those

TABLE V. Comparison between the experimental and theoretical rotational constants, methyl torsional parameters, barriers, and angles of the acetyl (upper) and methoxy (lower) methyl rotors of AAME. Theoretical values are specified as differences (Expt.–Calc.) relative to experiment.

| | Expt. ^a | MP2 ^b | B3LYP ^b | PW91 ^c | HCTH ^c |
|--|--------------------|------------------|--------------------|---------------------|--------------------|
| <i>A</i> (MHz) | 2998.4(3) | −16.1 | +54.6 | +114.0 | +138.6 |
| <i>B</i> (MHz) | 669.6(4) | −5.6 | +2.4 | +3.1 | +5.2 |
| <i>C</i> (MHz) | 596.6(3) | −2.9 | +1.6 | +1.3 | −1.8 |
| θ_a (°) ^d | 44.9(1) | +1.9 | +2.1 | +1.9 | +3.1 |
| θ_b (°) ^d | 46.7(1) | −1.4 | −1.8 | −1.4 | −2.9 |
| θ_c (°) ^d | 80.5(1) | −1.4 | −1.0 | −1.5 | −0.4 |
| V_3 (cm ^{−1}) | 65.6(7) | −2.7 | +20.1 | −22.2 ^e | −52.6 ^e |
| θ_a (°) ^d | 23.7(1.2) | −2.8 | −2.0 | −2.9 | −1.2 |
| θ_b (°) ^d | 66.5(1.2) | +3.0 | +2.2 | +3.1 | +1.4 |
| θ_c (°) ^d | 86.7(3) | −1.6 | −3.1 | −3.2 | −2.2 |
| V_3 (cm ^{−1}) | 399.2(3.0) | +0.3 | −145.6 | +166.3 ^e | +99.9 ^e |
| φ (°) | | −159.4 | −155.5 | −153.3 | −150.8 |
| ψ (°) | | 171.1 | 169.8 | 169.2 | 166.9 |
| $r_{\text{N-H}\cdots\text{O}=\text{C}}$ | | 2.218 | 2.239 | 2.234 | 2.291 |
| $\theta_{\text{N-H}\cdots\text{O}=\text{C}}$ | | 105.4 | 105.2 | 105.7 | 103.9 |

^aAverage of the JB95 and global fit methods with uncertainties representing one-half the difference in the values.

^bMP2 and B3LYP make use of the cc-pVTZ basis set and the GAUSSIAN03 program suite (Ref. 22).

^cPW91 and HCTH hybrid functionals make use of a double numerical basis and DMOL3 program suite (Ref. 3).

^dFor the theoretical values, the methyl top angles are taken from the center of gravity of the three methyl hydrogens to the Cartesian position of the methyl carbon.

^eZero-point energy corrections obtained from B3LYP/cc-pVTZ results (see Table VIII).

determined from the x-ray structural data, the *A*, *B*, and *C* constants are underestimated on average by 4.5%, 1.5%, and 1.2%, respectively, differences that are remarkably similar to those found here in the gas phase. It is apparent from these gas-phase comparisons that the structural errors in the monomers at least partially explain the discrepancies with the x-ray data since expanding the size of the monomers for a fixed cell volume would lead to hydrogen bonds that are too short.

Similar trends in the rotor axis angle differences, $\Delta\theta$, are not as apparent for the different levels of theory. For the acetyl methyl rotors of AAME and AAMA, the $\Delta\theta_a$ from MP2 and DFT are all positive while $\Delta\theta_c$ are always negative. Similarly, for the amide rotor of AAMA, $\Delta\theta_a$ and $\Delta\theta_b$ are positive while $\Delta\theta_c$ are negative at both levels. In contrast, $\Delta\theta_a$ and $\Delta\theta_c$ of the amide rotor of AAMA are of the same sign at the DFT level but opposite to that found at the MP2 level. While these differences are all less than 4°, it is interesting to note that the angle errors are of similar magnitude to the theoretical differences in the Ramachandran angles given in the lower parts of Tables V and VI. However, to draw any further conclusions, additional experimental structural data from isotopologues would first be necessary.

D. Torsional barrier comparisons

The torsional barriers reflect competing steric and hyperconjugative interactions with the orbitals adjacent to the methyl group and will be discussed in a forthcoming article.³⁰ Our general focus here is on the magnitudes of the predicted versus experimental barriers and the explicit impact of two

factors: the zero-point energy contributions and the next higher-order Fourier component, V_6 , in the torsional potential which is addressed separately below.

For a complete theoretical treatment of the methyl torsional barrier, the explicit definition of the symmetry adapted torsional coordinate in terms of the structure becomes an issue.^{31–33} However, for V_3 barrier calculations, the specification of the explicit coordinate is not relevant since no structural constraints were applied for either the equilibrium or transition state (top-of-barrier) calculations. The torsional barriers were calculated in a two step procedure. First, the methyl group was rotated by 180° and the structure was optimized except for the frozen dihedral defining the torsional coordinate. Then, fully relaxed geometries were obtained following optimization of the transition state structures. In all cases, a harmonic normal mode analysis revealed a single imaginary frequency. In the first approximation, a fair estimate of the V_3 term is the energy difference between the transition state and equilibrium structures. However, the experimentally determined barrier also includes contributions from the differences in the zero-point energies (ΔZPE) along the other normal mode coordinates, q_i , i.e.,

$$\langle \psi^*(q_1) \cdots \psi^*(q_{3n-6}) | \frac{1}{2} V_3(q_1, \cdots, q_{3n-6}) [1 - \cos(3\varphi)] \times | \psi(q_1) \cdots \psi(q_{3n-6}) \rangle, \quad (1)$$

where φ is the methyl torsional angle. Assuming an adiabatic separation of the torsional coordinate from the other vibrational degrees of freedom in Eq. (1),³³ the ΔZPE correction from theory requires identification of the methyl torsional mode in both the equilibrium and top-of-barrier configurations. While easily identified for the transition state structure

TABLE VI. Comparison between the experimental and theoretical rotational constants, methyl torsional parameters, barriers, and angles of the acetyl (upper) and amide (lower) methyl rotors of AAMA. Theoretical values are specified as differences relative to experiments as (Expt.–Calc.).

| | JB95 | MP2 ^a | B3LYP ^a | PW91 ^b | HCTH ^b |
|--|----------------------|------------------|--------------------|----------------------|----------------------|
| <i>A</i> (MHz) | 1711.0(5) | +4.7 | +6.8 | +17.3 | +0.7 |
| <i>B</i> (MHz) | 991.9(5) | −17.0 | +9.0 | +5.1 | +40.0 |
| <i>C</i> (MHz) | 716.1(5) | −10.5 | +7.6 | +10.1 | +15.6 |
| θ_a (°) ^c | 34.3(1) | +0.9 | +2.5 | +4.0 | +2.8 |
| θ_b (°) ^c | 82.3(1) | +1.2 | +0.7 | −0.8 | −1.2 |
| θ_c (°) ^c | 56.8(1) | −1.3 | −2.8 | −3.9 | −2.5 |
| V_3 (cm ^{−1}) | 98.5(1) ^d | −2.6 | +7.8 | −32.0 ^e | +38.2 ^e |
| θ_a (°) ^c | 47.4(1) | −0.9 | +0.5 | −0.2 | +1.3 |
| θ_b (°) ^c | 48.7(1) | +0.2 | −0.1 | +0.6 | −0.9 |
| θ_c (°) ^c | 71.0(1) | +1.2 | −0.6 | −0.6 | −0.7 |
| V_3 (cm ^{−1}) | 81.6(1) ^d | +32.2 | +55.1 ^e | +33.5 ^{e,f} | +54.2 ^{e,f} |
| φ (°) | | −82.5 | −83.8 | −83.0 | −88.1 |
| ψ (°) | | 74.9 | 73.3 | 70.8 | 76.4 |
| $r_{\text{N-H}\cdots\text{O}=\text{C}}$ | | 2.005 | 2.073 | 1.995 | 2.238 |
| $\theta_{\text{N-H}\cdots\text{O}=\text{C}}$ | | 145.4 | 144.2 | 147.5 | 142.3 |

^aMP2 and B3LYP make use of the cc-pVTZ basis set and the GAUSSIAN03 program suite (Ref. 22).

^bPW91 and HCTH hybrid functionals make use of a double numerical basis and the DMOL3 program suite (Ref. 3).

^cFor the theoretical values, the methyl top angles are taken from the center of gravity of the three methyl hydrogens to the Cartesian position of the methyl carbon.

^d V_3 barriers recalculated with fixed values of $F=5.30$ cm^{−1} for both rotors compared to values reported in Ref. 4.

^eConformational minimum *anti* and opposite to the MP2 (and HF) result.

^fZero-point energy corrections obtained from the B3LYP/cc-pVTZ results (see Table VIII).

as the mode with imaginary frequency, this vibration is often mixed with other modes in the equilibrium normal mode analysis. Methods making use of the intrinsic reaction coordinate³¹ or distinguished reaction coordinate³³ have been recently shown to resolve this problem. However, as a less computationally intensive alternative, an approximate ZPE corrected torsional barrier, V_3^{ZPE} , may be obtained from

$$V_3^{\text{ZPE}} = V_3 + \Delta\text{ZPE}_{\text{NT}} + \text{ZPE}_{\varphi} = V_3 + \Delta\text{ZPE},$$

where $\Delta\text{ZPE}_{\text{NT}}$ is the ZPE difference between the transition state (that excludes the mode with imaginary frequency) and the equilibrium geometry and ZPE_{φ} is that calculated di-

rectly for a $\frac{1}{2}V_3[1-\cos(3\varphi)]$ potential and a methyl rotor constant of $F=5.30$ cm^{−1}. The V_3^{ZPE} obtained in this way as well as the conformational preferences predicted for AAMA and AAME are summarized in Table VII. Unfortunately, the numerical nature of the DFT methods implemented in DMOL3 precluded a similar zero-point energy analysis. Therefore, the ΔZPE corrections applied in Tables V and VI for the PW91 and HCTH functionals are those from B3LYP/cc-pVTZ given in Table VII. We also include as a footnote in Table VII the V_3 torsional barriers calculated for the methyl rotors attached to the alanine residues of AAME and AAMA. Both barriers are larger than >1000 cm^{−1} and, therefore, are ex-

TABLE VII. Theoretical values of V_3 torsional barriers corrected for zero-point energy differences (ΔZPE). See text for method and definition of terms.

| | | Acetyl–Expt. V_3 65.6(7) cm ^{−1} | | | Methoxy–Expt. V_3 399.2(3.0) cm ^{−1} | | | |
|-------------------|--------------|---|--------------------|--------------------|---|-------|--------------------|--------------------|
| AAME ^a | ^b | V_3 | ΔZPE | V_3^{ZPE} | ^b | V_3 | ΔZPE | V_3^{ZPE} |
| HF/cc-pVTZ | <i>a</i> | 28.6 | −28.7 | −0.1 | <i>a</i> | 438.2 | −8.6 | 429.6 |
| B3LYP/cc-pVTZ | <i>a</i> | 84.3 | −35.8 | 45.5 | <i>a</i> | 262.6 | −9.0 | 253.6 |
| MP2/cc-pVTZ | <i>a</i> | 91.7 | −23.4 | 68.3 | <i>a</i> | 404.5 | −5.6 | 398.9 |
| | | Acetyl–Expt. V_3 98.5(1) cm ^{−1} | | | Amide–Expt. V_3 81.6(1) cm ^{−1} | | | |
| HF/cc-pVTZ | <i>a</i> | 45.1 | −29.4 | 15.7 | <i>s</i> | 122.6 | 10.8 | 133.4 |
| B3LYP/cc-pVTZ | <i>a</i> | 114.6 | −23.9 | 90.7 | <i>a</i> | 51.5 | −25.0 | 26.5 |
| MP2/cc-pVTZ | <i>a</i> | 126.5 | −25.4 | 101.1 | <i>s</i> | 49.6 | −0.1 | 49.5 |

^aThe V_3 torsional barriers calculated at the MP2/cc-pVTZ level for the methyl rotors on the alanine residues are 1266 and 1100 cm^{−1} for AAME and AAMA, respectively.

^bApproximate *anti* (*a*) or *syn* (*s*) equilibrium configurations of the methyl group with respect to the C=O bond for the acetyl and methoxy rotors and the N–H bond for the amide rotor.

TABLE VIII. Experimental determinations of V_3 from the spectral data that include fixed values of V_6 determined from least-squares fits to the relaxed potential energy surfaces calculated at the MP2/c-pVTZ and B3LYP/cc-pVTZ levels of theory for AAME. Results have been rounded to 0.1 MHz for clarity.

| | AAME | | | | | |
|--------|---------|-------------|-------------|----------|-------------|--------------|
| | Acetyl | | | Methoxy | | |
| | V_3^a | V_3/V_6^b | Δ | V_3^a | V_3/V_6^b | Δ |
| B3LYP | 84.3 | 83.9(2) | -0.4 | 262.6 | 264.5(5) | +1.9 |
| Global | 65.0(1) | 67.1(1) | +2.1 | 396.4(1) | 384.8(1) | -11.6 |
| JB95 | 66.3(1) | 68.3(1) | +2.0 | 402(4) | 391(4) | -11 |
| MP2 | 91.7 | 93.0(2) | +1.3 | 404.5 | 406.7(7) | +2.2 |
| Global | 65.0(1) | 69.3(1) | +4.3 | 396.4(1) | 385.2(1) | -11.2 |
| JB95 | 66.3(1) | 70.2(1) | +3.9 | 402(4) | 391(4) | -11 |

^a V_3 term only. Calculated values were determined from the energy difference between the equilibrium and transition state structures and exclude zero-point energy corrections. The global and JB95 values are from spectral fits of V_3 only ($V_6=0$).

^bThe V_3 and V_6 terms of $E=V_3/2[1-\cos(3\varphi)]+V_6/2[1-\cos(6\varphi)]$ were fitted to the B3LYP and MP2 relaxed potential energy torsional surfaces where φ is defined as the methyl torsional angle. The V_6 terms obtained from the B3LYP/MP2 surfaces were -6.7(2)/-13.6(2) and +15.5(6)/+15.0(7) for the acetyl and methoxy rotors, respectively. For the global and JB95 values, the V_6 terms were kept fixed to these quantum chemical values while V_3 was floated.

pected to have torsional splitting too small to be resolved in the MW region as observed.

After correction of the ΔZPE at the MP2 level, the torsional barriers for three of the four low-barrier tops are in excellent agreement with experiment while the barrier predicted for the amide rotor is still somewhat underestimated. Notice also that the effect of ΔZPE is less than 1/10 of the V_3 barriers for the methoxy and amide methyl rotors while contributions are more significant for the acetyl rotors amounting to as much as 1/3 of V_3 . At the DFT levels, no clear trends with the different functionals are evident where discrepancies are seen to vary by 8% in the best case and up to 80% (too high or low) in the other cases. One of the more surprising results is the near *anti* conformational minima predicted for amide methyl rotor of AAMA at all levels of DFT in contrast to the near *syn* minima predicted at the MP2 (and HF) level. This trend is found to be generally true for amide rotors of other peptide mimetics³⁰ and reveals a potential serious limitation of DFT methods for structural studies of peptides.

A second source of error in the torsional barrier comparisons regards the torsional barrier determination from the MW data. With only the ground state torsional level fit, the MW results give a measure of the V_3 term only in the potential energy surface. However, the next higher-order V_6 term in the Fourier expansion may also be important,³¹ i.e.,

$$E = \frac{1}{2}V_3[1 - \cos(3\varphi)] + \frac{1}{2}V_6[1 - \cos(6\varphi)],$$

where φ is the methyl torsional angle. To gain some insight into the impact of the V_6 term, relaxed potential surface scans were performed at the MP2 and B3LYP levels for AAME and the V_3 and V_6 terms were fitted to the resulting surfaces. A summary of the parameters is given in Table VIII and the contributions from each of these terms are shown separately in Fig. 5. Notice that at both levels of theory, the V_6 terms have opposite signs for the two different rotors and for the low barrier case, the form of the potential is signifi-

cantly improved with the addition of the V_6 term.

The V_6 contributions obtained in this way were then included as fixed parameters in the global and JB95 programs used to refit the V_3 terms to the spectroscopic data. The new values of the V_3 barriers are given in Table VIII. The effect of the V_6 terms is to increase V_3 of the acetyl rotor by only $\approx 2-4$ cm^{-1} and decrease V_3 of the methoxy rotor by ≈ 11 cm^{-1} at the B3LYP and MP2 levels. Therefore, the overall impact on the methyl torsional barriers is small and on the order of 6% for the acetyl rotors and decreases to 3% for the methoxy rotor. It is apparent from comparisons with results in Table VII that the ΔZPE corrections for the acetyl rotors are much more significant than the V_6 contributions.

V. CONCLUSION

For a number of protected dipeptides (with their C- and N-termini methyl capped) including alanine dipeptide,¹⁴ tryptophan,³⁴ and phenylalanine³⁵ studied in the gas phase, it has been found experimentally (and confirmed by high level *ab initio* calculations) that the lowest energy conformer is the γ -type secondary structure containing a hydrogen bond in a seven-atom ring (name C_7) from the amine to the carbonyl oxygen. In larger peptides, other phenomenon compete with γ turns: β turns bridging the backbone CO and NH groups via a ten-atom ring (C_{10}). Recent gas-phase studies employing UV and IR techniques in free-jet expansions have been used to isolate each conformation in order to study this competition between local conformational structures in tripeptides.³⁶ Fourier transform microwave spectroscopy coupled with high level quantum theory can give precise and complementary information regarding conformational structure. In this study, the substitution of the methyl amide group -[CONH]-CH₃ of AAMA by the methyl ester group C(=O)-O-CH₃ of AAME has interrupted the formation of the seven-atom ring intramolecular hydrogen bond arrangement observed for AAMA. Hence, the lowest energy conformer of AAME determined here is stabilized by an in-

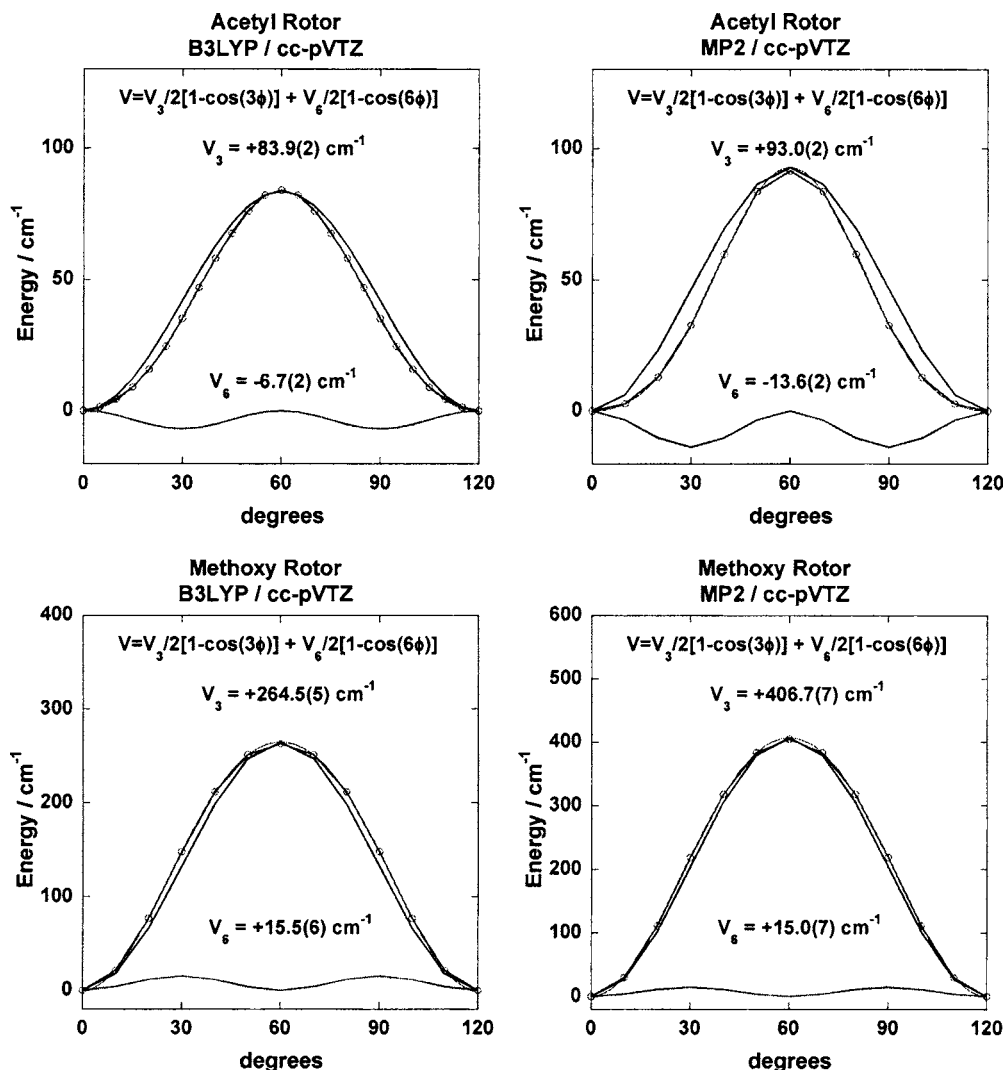


FIG. 5. Relaxed potential surface scans along the methyl torsional coordinate of the acetyl (top) and methoxy (bottom) groups at the B3LYP/cc-pVTZ (left) and MP2/cc-pVTZ (right) levels of theory. The best fit surfaces that include V_3 and V_6 contributions are shown superimposed.

tramolecular hydrogen bond from the amide proton of the [NHCO]-group to the carbonyl oxygen of the $\text{CH}_3\text{-O-C(=O)}$ group through a five-atom ring or C_5 interaction.

We have also demonstrated the application of one-top methods to analyze a two-top molecule, with different barrier heights and with neglect of top-top interactions. However, some care must be used when dealing with the structural information deduced (such as the methyl orientation angles) as there is some indeterminacy associated with the torsional parameters obtained from our fits when the barrier is high and the tunneling splittings carry little information. In further studies, two-top models⁹ should be applied to test the validity of our approximations that neglect the interaction between the two tops. One may also want to improve the uncertainties related to the torsional parameters by studying excited torsional states.

ACKNOWLEDGMENTS

The authors are deeply indebted to Dr. J. T. Hougen for numerous discussions and advice during the course of this

study and preparation of this manuscript. One of the authors (I.K.) would like to thank the “Institut du Développement et des Ressources en Informatique Scientifique” (IDRIS) for allocation of computer time.

¹A. D. MacKerell, Jr., *J. Comput. Chem.* **25**, 1584 (2004).

²H. Guo, S. Sirois, E. I. Proynov, and D. R. Salahub, in *Theoretical Treatment of Hydrogen Bonding*, edited by D. Hadzi (Wiley, Chichester, 1997).

³B. Delley, *J. Chem. Phys.* **92**, 508(1990); **113**, 7756 (2000).

⁴V. N. Staroverov, G. E. Scuseria, J. Tao, and J. P. Perdew, *J. Chem. Phys.* **119**, 12129 (2003); R. Improta and V. Barone, *J. Comput. Chem.* **25**, 1333 (2004).

⁵K. Siegrist, C. R. Bucher, I. Mandelbaum, A. R. Hight Walker, R. Balu, S. K. Gregurick, and D. F. Plusquellic, *J. Am. Chem. Soc.* **128**, 5764 (2006).

⁶R. D. Brown, P. D. Godfrey, and B. Kleibomer, *J. Mol. Spectrosc.* **124**, 34 (1987).

⁷V. V. Ilyushin, E. A. Alekseev, S. F. Dyubko, I. Kleiner, and J. T. Hougen, *J. Mol. Spectrosc.* **227**, 115 (2004).

⁸A. Fantoni, W. Caminati, H. Hartwig, and W. Stahl, *J. Mol. Struct.* **612**, 305 (2002).

⁹N. Ohashi, J. T. Hougen, R. D. Suenram, F. J. Lovas, Y. Kawashima, M. Fujitake, and J. Pyka, *J. Mol. Spectrosc.* **227**, 28 (2004).

¹⁰N. Heineking and H. Dreitzler, *Z. Naturforsch., A: Phys. Sci.* **48**, 570 (1993).

- ¹¹ Y. Kawashima, R. D. Suenram, and E. Hirota, *J. Mol. Spectrosc.* **219**, 105 (2003).
- ¹² B. Bakri, J. Demaison, I. Kleiner, L. Margulès, H. Møllendal, D. Petitprez, and G. Włodarczak, *J. Mol. Spectrosc.* **215**, 312 (2002).
- ¹³ R. J. Lavrich, A. R. Hight Walker, D. F. Plusquellic, I. Kleiner, R. D. Suenram, J. T. Hougen, and G. T. Fraser, *J. Chem. Phys.* **119**, 5497 (2003).
- ¹⁴ R. J. Lavrich, D. F. Plusquellic, R. D. Suenram, G. T. Fraser, A. R. Hight Walker, and M. J. Tubergen, *J. Chem. Phys.* **118**, 1253 (2003).
- ¹⁵ R. J. Lavrich, D. F. Plusquellic, R. D. Suenram, G. T. Fraser, A. R. Hight Walker, and M. J. Tubergen (unpublished).
- ¹⁶ I. Kleiner and J. T. Hougen, *J. Chem. Phys.* **119**, 5505 (2003).
- ¹⁷ R. D. Suenram, J.-U. Grabow, A. Zuban, and I. Leonov, *Rev. Sci. Instrum.* **70**, 2127 (1999).
- ¹⁸ W. A. Majewski, J. F. Pfanstiel, D. F. Plusquellic, and D. W. Pratt, in *Laser Techniques in Chemistry*, edited by A. B. Myers and T. R. Rizzo (Wiley, New York, 1995), Vol. XXIII, pp. 101–148; D. F. Plusquellic, R. D. Suenram, B. Mate, J. O. Jensen, and A. C. Samuels, *J. Chem. Phys.* **115**, 3057 (2001).
- ¹⁹ C. C. Lin and J. D. Swalen, *Rev. Mod. Phys.* **31**, 841 (1959).
- ²⁰ B. N. Taylor and C. E. Kuyatt, NIST Tech. Note 1297, (1993). The publication may be downloaded from <http://physics.nist.gov/Pubs/guidelines/contents.html>
- ²¹ See EPAPS Document No. E-JCPSA6-125-009636 for the assignments, observed values, and residuals obtained from the C_1 -RAM global fit for the measured microwave transitions of the (*AA*,*EA*) state (acetyl rotor, Table I) and (*AA*,*AE*) state (methoxy rotor, Table II) of AAME. This document can be reached via a direct link in the online article's HTML reference section or via the EPAPS homepage (<http://www.aip.org/pubservs/epaps.html>).
- ²² M. J. Frisch, G. W. Trucks, H. B. Schlegel *et al.*, GAUSSIAN03, Revision B.04, Gaussian Inc., Pittsburgh, PA, 2003.
- ²³ A. D. Becke, *J. Chem. Phys.* **98**, 5648 (1993).
- ²⁴ C. T. Lee, W. T. Yang, and R. G. Parr, *Phys. Rev. B* **37**, 785 (1988).
- ²⁵ A. G. Baboul, L. A. Curtiss, P. C. Redfern, and K. Raghavachari, *J. Chem. Phys.* **110**, 7650 (1999).
- ²⁶ C. Møller and M. S. Plesset, *Phys. Rev.* **46**, 618 (1934).
- ²⁷ T. H. Dunning, Jr., *J. Chem. Phys.* **90**, 1007 (1989); D. E. Woon and T. H. Dunning, Jr., *ibid.* **98**, 1358 (1993).
- ²⁸ J. P. Perdew and Y. Wang, *Phys. Rev. B* **45**, 13244 (1992).
- ²⁹ J. P. Perdew, K. Burke, and M. Ernzerhof, *Phys. Rev. Lett.* **77**, 3865 (1996).
- ³⁰ D. F. Plusquellic and D. W. Pratt (unpublished).
- ³¹ L.-H. Xu, R. M. Lees, and J. T. Hougen, *J. Chem. Phys.* **110**, 3835 (1999); L. H. Xu, J. T. Hougen, R. M. Lees, and M. A. Mekhtiev, *J. Mol. Spectrosc.* **214**, 175 (2002).
- ³² T. V. Albu and D. G. Truhlar, *J. Mol. Spectrosc.* **219**, 129 (2003).
- ³³ V. Szalay, A. G. Császár, and M. L. Senent, *J. Chem. Phys.* **117**, 6489 (2002); W. D. Allen, A. Bodi, V. Szalay, and A. G. Császár, *ibid.* **124**, 224310 (2006).
- ³⁴ B. C. Dian, A. Longarte, and T. S. Zwier, *Science* **296**, 2369 (2002).
- ³⁵ M. Gerhards, C. Unterberg, A. Gerlach, and A. Jansen, *Phys. Chem. Chem. Phys.* **6**, 2682 (2004).
- ³⁶ W. Chin, M. Mons, J.-P. Dognon, F. Piuze, B. Tardivel, and I. Dimicoli, *Phys. Chem. Chem. Phys.* **6**, 2700 (2004).